Stability and accuracy analysis of the space-frequency domain wavefield extrapolators

Kun Liu, Hugh D. Geiger, John C. Bancroft and Gary F. Margrave

ABSTRACT

Space-frequency domain wavefield extrapolators have attractive advantages compared to wavenumber-frequency domain extrapolators. The most attractive merit is that they can accurately handle strong lateral velocity variations without incurring a significant increase in computational cost. It is well-known that finite space-frequency domain extrapolators are designed as approximations to the exact phase-shift operator. These approximations manifest themselves as small instabilities and inaccuracies in the performance of the extrapolators. These effects are best examined in the wavenumber-frequency domain, where the extrapolator response can be compared to the exact response, and in the space-time domain, where angular aperture, wavelet stability, and artifacts can be evaluated and compared. In this paper, we compare the 19- and 39-point Hale, Nautiyal (Gaussian tapered), and Kirchhoff (Hanning tapered) extrapolators. We use a common set of standards to visualize the various extrapolators and quantitatively investigate their stability and accuracy. The dip responses of the extrapolators are compared using constant velocity 2-D impulse responses (zero-offset) and a constant velocity pre-stack depth migration of a single shot-record over a carefully designed set of dipping reflectors.

INTRODUCTION

In recent years, "wave equation" seismic imaging methods have found wider application as computational power has steadily increased and as exploration efforts target areas with strong lateral variations in seismic velocity. The essential component of a "wave equation" imaging method is recursive wavefield extrapolation based on the one-way wave equation (Berkhout, 1981), where the term recursive implies that the output wavefield from the last extrapolation step is used as the input wavefield to the next extrapolation step. Various "wave equation" imaging methods have demonstrated a superior capability for imaging complex structures compared to conventional nonrecursive methods typified by diffraction-stack Kirchhoff migration (Paffenholz et al., 2002; Soubaras, 2002). A widely agreed explanation is that recursive extrapolators provide an accurate solution to the wave equation over the whole range of seismic frequencies. Therefore, they are more easily able to handle complex wave phenomena such as multiple arrivals and complicated scattering (Bevc and Biondi, 2002).

The recursive wavefield extrapolation methods can be categorized into two major groups, implicit and explicit. A typical example based on the implicit extrapolation is the well-known 45-degree finite-difference method for depth migration (Claerbout, 1985), where the implicit filtering is implemented by solving a linear system of coupled equations for the output points. In contrast, the explicit methods approximate the extrapolation operator as finite-length spatial filters. Recursive Kirchhoff extrapolation (Bevc, 1997; Margrave and Daley, 2001; Geiger et al., 2002) and the family of wavenumber-frequency extrapolations such as phase-shift-plus-interpolation (Gazdag and

Sguazerro, 1984) and non-stationary phase shift (Margrave and Ferguson, 1999; Ferguson and Margrave, 2002) are considered to be explicit methods.

One compelling advantage of explicit methods is the ease with which they can be coded for parallel implementation (e.g., Geiger et al., 2002) and extended to the 3-D case (Claerbout, 1985). Moreover, explicit extrapolation methods implemented in the space-frequency domain (e.g., the recursive Kirchhoff extrapolation) can easily handle irregular acquisition geometry (Margrave and Daley, 2001) and provide protection from wrap-around artifacts that typically appear with wavenumber-frequency extrapolators.

Although these are desirable advantages, stability and accuracy are always major concerns when designing explicit extrapolation schemes implemented in the space-frequency domain. Unlike implicit extrapolations, which are unconditionally stable (Godfrey et al., 1979; Claerbout, 1985), explicit extrapolators are not stable unless special care is taken in their design and implementation. In general, instability results from spatial truncation of the explicit extrapolation operators, either for the purpose of decreasing the computational cost or due to the inevitable finite aperture of the survey. Specifically, truncation of the spatial aperture of extrapolators causes a Gibbs oscillation in the wavenumber domain, and instability arises when any part of the amplitude spectrum exceeds one. Recursive application of the truncated extrapolator tends to amplify the wavefield energy with depth, damaging the final images. In other words, the stability condition that no amplitude at any frequency will grow exponentially with depth is not automatically fulfilled with explicit extrapolators. The other important factor is accuracy, which could be comprised if the amplitude and phase spectra of the extrapolator deviate from those of the exact analytical phase-shift operator.

Many efforts have been devoted to stabilize the space-frequency domain extrapolators without sacrificing accuracy. Holberg (1988) and Blacquière et al. (1989) suggested a constrained non-linear least-square method to design 2-D and 3-D stable extrapolators, respectively. Unfortunately, as shown by Hale (1991), the recursive application of non-linear least-square optimized extrapolators may still result in instability and/or exponential decay of the seismic wavefield with depth. In addition, the nonlinear algorithm is usually expensive and can be trapped in a local minimum (Thorbecke et al., 2004). As an alternative, Hale proposed a stable explicit extrapolator designed using a modified Taylor series method. Although Hale's extrapolator is guaranteed to be stable, the artifacts caused by the nature of the extrapolator design make it suboptimal (see following discussion). An additional drawback is that Hale's method is based on the Taylor series expansion about wavenumber zero. Therefore, it's no longer accurate to handle propagation angles at high wavenumbers. A more straightforward way to stabilize the extrapolator as well as accommodate the irregular geometry is to taper the extrapolator in the space domain by multiplying a proper window function. A successful example was shown by Nautiyal et al. (1993) using a Gaussian window. However, as seen later, its abilities to image the steep dips and keep phase accurate are not competitive with Hale's extrapolator. Other extrapolators were also designed that demonstrated interesting stability and accuracy features, e.g., Soubaras (1996) suggests equiripple polynomial expansion combined with Laplacian synthesis, while Thorbeck et al. (1994 and 2004) suggest an optimized weighted least-squares method.

The criteria for an optimal space-frequency domain extrapolator would mainly rely on the specific stability and accuracy analysis, where deep insights should be gained in order to make the fair comparison. To date, there has not been a study that compares the accuracy and stability of various extrapolators using a common set of standards. In this paper, I developed an intuitive way to visualize the wavefield extrapolators and illustrate the stability and accuracy problems in the explicit wavefield extrapolation. This leads to a better understanding of the stability and accuracy problems, and a more effective evaluation of various explicit wavefield extrapolators. More importantly, it will pave the way for developing new wavefield extrapolation techniques.

It's hard to compare all the extrapolators that have been introduced in the literature. Instead, I selected recursive Kirchhoff extrapolator, Nautiyal's Gaussian tapered extrapolator and Hale's extrapolator to exemplify the stability and accuracy analysis. They are either widely referenced or well developed, thus, make themselves good candidates. Furthermore, in order to make the fair comparison, I coded Nautiyal's, Hale's and Kirchhoff extrapolators on a common platform[1].

In this paper, I briefly introduce the three extrapolation methods, followed by the stability and accuracy analysis. Post-stack and pre-stack synthetic data are used for the illustration.

EXPLICIT WAVEFIELD EXTRAPOLATORS

Hale's stable explicit extrapolator

Hale (1991) proposed a modified Taylor series method to stabilize the explicit wavefield extrapolator. The method can be viewed as the design of a finite length extrapolation filter $h(n)$ with a Fourier transform $H(\hat{k})$ that best approximates the Fourier transform $D(\hat{k})$ of the desired extrapolator,

$$D(\hat{k}) = \exp\left\{ i\left(\frac{\Delta z}{\Delta x}\right)\left[\left(\frac{\omega \Delta x}{v}\right)^2 - \hat{k}^2\right]\right\}, \qquad (1)$$

where ω denotes the angular frequency (in radians per unit time), v denotes velocity, and Δz and Δx denote vertical and horizontal spatial sampling intervals. The normalized wavenumber $\hat{k}$ (in radians per sample) is obtained by multiplying the wavenumber k by Δx. $D(\hat{k})$ is the familiar filter applied in Gazdag's (1978) phase-shift migration, and is subject to the constraint that $\left|H(\hat{k})\right| \le 1$ for $\left|\hat{k}\right| \le \pi$.

The desired transform $D(\hat{k})$ uniquely depends on the two dimensionless constants $\Delta z / \Delta x$ and $\omega \Delta x / v$. As indicated by equation (1), $D(\hat{k})$ is symmetric with respect to $\hat{k}$ (both the real and imaginary parts are even), which implies that $h(n)$ should also be even. Thus, the length of $h(n)$, measured by N, should be odd, with the coefficient index

[1] Kirchhoff extrapolator is revised from the existing algorithm by Margrave.

n bounded by $-(N-1)/2 \le n \le (N-1)/2$. Moreover, due to the symmetry of $h(n)$ it is completely described by *(N+1)/2* coefficients.

The extrapolation filter $h(n)$ is defined by

$$h(n) = \sum_{m=0}^{M-1} c_m b_{mn} \,, \tag{2}$$

where the basis function b_{mn} is chosen as

$$b_{mn} = (2 - \delta_{m0}) \cos\left(\frac{2\pi mn}{N}\right), \tag{3}$$

and δ_{mo} is the *Kronecker delta function* defined by

$$\delta_{m0} = \begin{cases} 1. \;\; if \; m = 0; \\ 0. \;\; otherwise. \end{cases} \tag{4}$$

To ensure stability of the extrapolator (i.e., $\left|H(\hat{k})\right| \le 1$), the number of weights M in equation (2) should be less than the number of filter coefficients *(N+1)/2*. The Fourier transform of $h(n)$ is obtained as

$$H(\hat{k}) = \sum_{m=0}^{M-1} c_m B_m(\hat{k}) \,, \tag{5}$$

where

$$B_m(\hat{k}) = (2 - \delta_{m0}) \sum_{n=0}^{(N-1)/2} (2 - \delta_{n0}) \cos\left(\frac{2\pi mn}{N}\right) \cos(\hat{k}n) \,. \tag{6}$$

The Taylor series expansion of the desired transform *D(k)* and the approximation $H(\hat{k})$ about 0 (i.e., the Maclaurin series) can be calculated respectively as

$$D(\hat{k}) = D(0) + D'(0)\hat{k} + \frac{D''(0)}{2!}\hat{k}^2 + \ldots + \frac{D^{(n)}(0)}{n!}\hat{k}^n + \ldots \,. \tag{7}$$

$$\begin{aligned} H(\hat{k}) &= H(0) + H'(0)\hat{k} + \frac{H''(0)}{2!}\hat{k}^2 + \ldots + \frac{H^{(n)}(0)}{n!}\hat{k}^n + \ldots \\ &= \sum_{m=0}^{M-1} c_m B_m(0) + \hat{k}\sum_{m=0}^{M-1} c_m B_m'(0) + \frac{\hat{k}^2}{2!}\sum_{m=0}^{M-1} c_m B_m''(0) + \ldots + \frac{\hat{k}^n}{n!}\sum_{m=0}^{M-1} c_m B_m^{(n)}(0) + \ldots . \end{aligned} \tag{8}$$

Since $D(\hat{k})$ and $H(\hat{k})$ are symmetric, the odd derivatives at $\hat{k} = 0$ in equation (7) and (8) are all zeros.

The conventional way to approximate $D(\hat{k})$ is to match the first *(N+1)/2* even derivatives at $\hat{k} = 0$ in equation (7), which can result in an unstable extrapolation filter. The instability arises when the amplitudes of $H(\hat{k})$ exceed one due to the truncation of the infinite Taylor series. Instead, Hale's suggests matching only the first M (for $M \le (N+1)/2$) even derivatives, yielding the linear system,

$$\sum_{m=0}^{M-1} c_m B_m^{(2l)}(0) = D^{(2l)}(0), \tag{9}$$

where,

$$B_m^{(2l)}(0) = \begin{cases} (2-\delta_{m0})\left[1+2\sum_{n=1}^{(N-1)/2}\cos\left(\frac{2\pi mn}{N}\right)\right] & (l=0) \\ 2(2-\delta_{m0})(-1)^l \sum_{n=1}^{(N-1)/2}\cos\left(\frac{2\pi mn}{N}\right)n^{2l} & (l=1,2,...,M-1) \end{cases}. \tag{10}$$

Note that Equation (10) has corrected an error in Hale's equation (A-6). The remaining *(N+1)/2-M* degrees of freedom are used to achieve the stability of the extrapolation filter. The weights c_m can be obtained from equation (9) by solving the linear system. The extrapolation filter *h(n)* is then obtained from equation (2).

In practice, we consider an extrapolator to be stable when its amplitude is smaller than 1.0001 for all wavenumbers. In a homogenous medium and a single frequency, the amplitude will be amplified to a maximum value of 1.1052 after 1000 extrapolation steps. This is considered as being "reasonably" stable.

Recursive Kirchhoff extrapolator

If $\psi(x, y, z=0, \omega)$ is a wavefield in the space-frequency (x, y, ω) domain at depth level $z = 0$, then its extrapolated value at depth z is calculated as

$$\psi(x, y, z, \omega) = \int_{-\infty}^{\infty} \psi(\hat{x}, \hat{y}, z=0, \omega) W_{3D}(x-\hat{x}, y-\hat{y}, z, v, \omega) d\hat{x} d\hat{y}, \tag{11}$$

where v is the laterally variable velocity and W_{3D} is the three-dimensional, space-frequency, wavefield extrapolation operator. It can be derived by taking the z derivative of 3-D Green's function for constant velocity, i.e.

$$W_{3D}(x, y, z, v, \omega) = -\frac{ik\cos\theta}{2\pi r} e^{ikr}\left(1+\frac{i}{kr}\right), \tag{12}$$

where $r = \sqrt{x^2+y^2+z^2}$, $k = \omega / v$ and $\cos\theta = z/r$ is the cosine of the scattering angle.

By substituting equation (12) into equation (11), we obtain

$$\psi(x,y,z,\omega)=\frac{-i\omega}{2\pi}\int_{-\infty}^{\infty}\psi(\hat{x},\hat{y},z=0,\omega)\frac{z}{v\tilde{r}^{2}}e^{i\omega\tilde{r}/v}\left(1+\frac{iv}{\omega\tilde{r}}\right)d\hat{x}d\hat{y}\,, \tag{13}$$

where $\tilde{r}=\sqrt{(x-\hat{x})^2+(y-\hat{y})^2+z^2}$. Equation (13) is a spatial convolution of the wavefield with an operator that performs a weighted summation along a diffraction curve. Therefore, equation (13) is interpretable as a Kirchhoff-style wavefield extrapolation operation in the space-frequency domain (Margrave and Daley, 2001). Depending on the choice of Fourier transform convention, W_{3D} can represent either a forward or backward wavefield extrapolation operator.

The Kirchhoff extrapolator is different from typical space-frequency extrapolators (e.g., Berhout (1981)). The traditional space-frequency extrapolators are usually designed as finite-difference operators and thus assume a uniformly gridded dataset. The Kirchhoff extrapolator, on the other hand, is derived from an analytical formula that can be evaluated at any arbitrary spatial location. Therefore, it can easily adapt to irregular geometry and could prove effective in data regularization.

Similarly, the 2-D form of wavefield extrapolation can be developed as,

$$\psi(x,z,\omega)=\frac{i\omega}{2}\int_{-\infty}^{\infty}\psi(\hat{x},z=0,\omega)\frac{\cos\theta}{v}H_1^{(1)}\left(\frac{\omega\tilde{\rho}}{v}\right)d\hat{x} \tag{14}$$

where $H_1^{(1)}(u)$ is the first-order Hankel function of the first kind and $\tilde{\rho}=\sqrt{(x-\hat{x})^2+z^2}$.

The simple replacement of constant velocity by lateral variable velocity in equation (13) and (14) leads to the extrapolators that can approximately accommodate lateral velocity variations.

Nautiyal's Gaussian tapered extrapolator

Nautiyal (1993) suggested applying a Gaussian window,

$$T(x)=e^{(-\frac{x^2}{2\sigma^2})}\,, \tag{15}$$

to the Kirchhoff extrapolator in the space-frequency domain. σ is a parameter to be chosen. Spatial tapering by a Gaussian window is easy to implement and stabilizes the extrapolator.

STABILITY AND ACCURACY ANALYSIS

The space-frequency domain extrapolators studied in this paper are plotted in the wavenumber-frequency domain so that a direct comparison can be made with the exact phase-shift extrapolator for constant velocity. A constant velocity of 1250m/s (half-velocity of 2500m/s for zero-offset extrapolation), frequency range of 0 to 55Hz, spatial sampling of Δx=Δz=10m and temporal sampling of 4ms are used for the extrapolators calculation. To be consistent with the literature (e.g., Hale (1991) and Nautiyal (1993)), the operator lengths used in the demonstration are chosen as 19 and 39 points.

As illustrated in Figure 1 and 3, the various explicit extrapolators implemented in the space-frequency domain are designed in different ways to approximate the desired phase-shift operator. Figure 1(a) and 3(a) are the spectra of the desired extrapolator (phase-shift operator) obtained from equation (1). Wavenumbers and phase are normalized by the factors of $2\pi/\Delta x$ and 2π, respectively. The full-aperture Kirchhoff extrapolator (Figure 2(a) and 4(a)) shows the smallest amplitude and phase errors in comparison to other "limited aperture" extrapolators[2]. However, there are number of reasons why full-aperture extrapolation is less desirable in practice. First, full-aperture extrapolation is computationally expensive, especially in 3-D. Second, the finite aperture in the space domain causes a Gibbs oscillation in the wavenumber domain with a resultant amplification or attenuation of portions of the wavefield. Therefore, limited aperture extrapolation can be, at best, only "reasonably" stable for a finite number of extrapolation steps. Third, it is important to note that, even at infinite aperture, we always choose to attenuate the evanescent region and are thus making errors for inverse extrapolation (see Wapenaar (1997)). Although tapering techniques have been shown to be effective in handling truncation problems (Liu et al., 2004), a simple Hanning edge taper in the space domain cannot stabilize the 19-point and 39-point Kirchhoff extrapolators. As indicated from in Figure 1(c) and 3(c), the Hanning edge taper is not able to guarantee that the amplitudes of extrapolators won't exceed one.

Both Hale's extrapolator (Figure 1(b) and 3(b)) and Gaussian tapered extrapolator (Figure 1(d) and 3(d)) are guaranteed to be stable without amplifying wavefield during the recursive extrapolation. However, differences in their design result in differences in accuracy. Taking advantage of the Gaussian window (the Fourier transform of the Gaussian is another Gaussian), Gaussian tapered extrapolator is like a "smoothed" version of the exact extrapolator where Gibbs oscillation is removed but high angle propagation energy is also attenuated. The fact that the phase error is not zero at small wavenumbers (Nautiyal (1993); Figure 2(d) and 4(d) in this paper) makes it less competitive. In contrast, Hale's extrapolator achieves better accuracy by matching the first few terms in Taylor series expansion of the exact extrapolator. As indicated by Figure 2(b) and 4(b), Hale's extrapolators are more accurate within the evanescent boundary. Unfortunately, the nature of the design for Hale's extrapolator will cause blocky spectra in the wavenumber-frequency domain (Figure 1(b) and 3(b)). As will see later, the discontinuities between each frequency bands will result in high-angle artifacts that could have been canceled out if there were energy in between the high wavenumber gaps. In addition, as Hale's extrapolator was derived from the Taylor series expansion at $k=0$, it won't be accurate to handle the high propagation angles. This is evident from the Figure 2(b) and 4(b) where the amplitude and phase errors increase with wavenumbers.

The above accuracy evaluation of various extrapolators is qualitative. A quantitative way is to investigate how the errors are associated with propagation angles. As depicted in Figure 5(a), one extrapolation step using Hale's 39-point extrapolator will attenuate the waves propagating at 55° by a factor of 0.995 (i.e., 1-1/200) for most frequencies. A 200-step extrapolation will attenuate the wave by a factor of $0.995^{200}=0.367$. Similarly, the

[2] Strictly speaking, "full-aperture" is also aperture-limited due to the finite acquisition survey. In this paper, the "limited aperture" refers to the case where the full-aperture is not used.

wave propagating at 70° will be attenuated by a factor of 0.95^{20}=0.359 only after 20 steps for many frequencies. This is a quantitative way to evaluate the ability of an extrapolator to propagate wavefields accurately over a range of propagation angles. Given that phase errors accumulate, the phase error contour shown by Figure 5(a) indicated that one-half cycle (π radians) phase error will be generated after 1000 step extrapolation for the waves propagating at 55°, while it only takes 100 steps for the waves propagating at 70°. Therefore, inaccurate waves are rapidly attenuated during the extrapolation.

As shown by Figure 5(b), the 39-point Kirchhoff extrapolator with Hanning edge taper is more accurate for most of frequencies. It will attenuate waves propagating at 60°-70° by a factor of 0.367 after 200 extrapolation steps (except the very low and high frequencies). A half cycle phase error will be generated after 1000 steps for the wave propagating at 70°-80° degrees. However, the 39-point Kirchhoff extrapolator with Hanning edge taper is not stable as described before. The 39-point Gaussian tapered extrapolator is probably the least accurate extrapolator as shown by Figure 5(c). It will attenuate waves propagating at 40° by a factor of 0.367 after 200 extrapolation steps (except for the very low and high frequencies).

SYNTHETIC TESTS

Zero-offset synthetic test

Zero-offset synthetic tests (impulse responses) are conducted with a half-velocity of 1250 m/s, receiver spread of 2000 m and maximum extrapolation depth of 2000 m. The spatial sampling is Δx=Δz=10 m and the temporal sampling is Δt=4 ms. A Ricker wavelet is seeded at t=0 with a dominant frequency of 24 Hz. As depicted by Figure 6, the impulse response from full-aperture Kirchhoff extrapolator is the best and will be used as the reference.

In general, the 19-point extrapolators (Figures 6(b), (c) and (d) on the left) are less accurate than the 39-point extrapolators (Figures 6(b), (c) and (d) on the right). The Hanning tapered Kirchhoff extrapolators (Figure 6(c)) preserve higher propagation angles than the other two extrapolators, but they start to become unstable – this is particularly noticeable with the 19 point Hanning extrapolator (Figure 6(c), on the left). As predicted by the error contours, the impulse response from Hale's 39-point extrapolator (Figure 6 (b), on the right) shows attenuation at about 55 degrees after 200 extrapolation steps. There are also artifacts present at high propagation angles caused by discontinuities in the extrapolator. Hale's 39-point extrapolator generates fewer artifacts than the 19-point extrapolator (Figure 6(b)) because the discontinuities in the 39-point extrapolator are less severe than those in the 19-point extrapolator. Gaussian tapered extrapolators have the poorest angular aperture of all tested extrapolators. (Figure 6(d)). This is not surprising in view of the amplitude error contours in Figure 5(c). Tapering by Gaussian window in the space domain is just a compromise between stability and accuracy.

Pre-stack synthetic test

A prestack synthetic test is used to examine the accuracy of pre-stack depth migration based on the wavefield extrapolators studied in this paper. The synthetic shot record (Figure 7(b)) is generated from the homogeneous model (v=2500 m/s) depicted in Figure

7(a). The spatial sampling is $\Delta x=\Delta z=10$ m and the temporal sampling is $\Delta t=4$ ms. The model contains 17 dipping reflectors at the dip angles of 0°, 10°, 20°, 30°, 40°, 50°, 60°, 70° and 80°. The position of each reflector is carefully chosen so that the normal to the center of the reflector projects through $x=0$. Thus the maximum dip imaged will provide a coarse quantitative measure of the angular aperture of both the forward propagating shot wavefield and the backward propagating receiver wavefield.

The migration results are shown in Figure 8, with the dipping reflectors superimposed on the left half of the figures. Again, the full-aperture migration yields the best result and is used as the reference. The migration based on the 39-point Hanning tapered Kirchhoff extrapolator yields a poor image (Figure 8(c)) with most of the reflectors incorrectly positioned. Even the horizontal reflector is poorly positioned due to phase rotation of the wavelet during propagation. Hale's 39-point extrapolator images reflectors up to a dip angle of 60° (Figure 8(b)). Noise in Figure 8(b) is a consequence of the notched design of Hale's extrapolator discussed previously. Figure 8(d) shows that a pre-stack depth migration based on the 39-point Gaussian tapered extrapolator is stable but less accurate. It only imaged the reflectors with a maximum dip angle of 30°. The phase is also deviated from the desired result (Figure 8(a)).

CONCLUSIONS

In this paper, we investigated the stability and accuracy of explicit space-frequency domain wavefield extrapolators. An intuitive visualization for various extrapolators is developed to help understand wavefield extrapolators and stability and accuracy problems. A comprehensive analysis is conducted by using error contouring, impulse responses and pre-stack synthetic test. It is expected that the tools developed in this paper will be utilized in evaluating the stability and accuracy of other wavefield extrapolators.

ACKNOWLEDGEMENTS

The authors would like to thank the sponsors of CREWES for financial support.

REFERENCES

Berkhout, A. J., 1981, Wave field extrapolation techniques in seismic migration, a tutorial: Geophysics, **46**, 1638-1656.

Bevc, D., 1997, Imaging complex structures with semirecursive Kirchhoff migration: Geophysics, **62**, 577-588.

Bevc, D., and Biondi, B., 2002, Which depth imaging method should we use? A road map in the maze of 3-D depth imaging: 72nd Ann. Internat. Mtg., Soc. of Expl. Geopohys., Expanded Abstracts, 1236-1239.

Blacquière, G., Debeye, H. W. J., Wapenaar, C. P. A., and Berkhout, A. J., 1989, 3D table-driven migration: Geophysical Prosepcting, **37**, 925-958.

Claerbout, J. F., 1985, Imaging the earth's interior: Blackwell Scientific Publications.

Ferguson, R. J., and Margrave, G. F., 2002, Prestack depth imaging by symmetric nonstationary phase shift: Geophysics, **67**, 594-603.

Gazdag, J., 1978, Wave equation migration with the phase shift method: Geophysics, **43**, 1342-1351.

Gazdag, J. and Sguazerro, P., 1984, Migration of seismic data by phase shift plus interpolation: Geophysics, **49**, 124-131.

Geiger, H. D., Margrave, G. F., Foltinek, D. S. and Langlois, J. M., 2002, Parallel 3D prestack depth migration using recursive Kirchhoff extrapolation: CREWES Research Report, **14**, 1-20.

Godfrey, R. J., Muir, F. and Claerbout, J. F., 1979, Stable extrapolation: SEP-16, 83-87.

Hale, D., 1991, Stable explicit depth extrapolation of seismic wavefields: Geophysics, **56**, 1770-1777.

Holberg, O., 1988, Towards optimum one-way wave propagation: Geophysical Prospecting, **36**, 99-114.

Liu, K., Geiger, H. D., Bancroft, J. C. and Margrave, G. F., 2004, Adaptive tapering in the wavefield extrapolation: 74th Ann. Internat. Mtg: Soc. of Expl. Geophys., MIG. 2.

Margrave, G. F. and Daley, P. F., 2001, Recursive Kirchhoff extrapolators: CREWES Research Report, **13**, 617-646.

Margrave, G. F. and Ferguson, R. J., 1999, Wavefield extrapolation by nonstationary phase shift: Geophysics, **64**, 1067-1078.

Nautiyal, A., Gray, S. H., Whitmore, N. D. and Garing, J. D., 1993, Stability versus accuracy for an explicit wavefield extrapolation operator: Geophysics, **58**, 277-283.

Paffenholz, J., Stefani, J., McLain, B. and Bishop, K., 2002, SIGSBEE_2A Synthetic Subsalt Dataset - Image Quality as Function of Migration Algorithm and Velocity Model Error: 64th Ann. Internat. Mtg.: Eur. Assn. Geosci. Eng., B019.

Soubaras, R., 1996, Explicit 3-D migration using equiripple polynomial expansion and Laplacian synthesis: Geophysics, **61**, 1386-1393.

Soubaras, R., 2002, Comparison of Kirchhoff and wave-equation prestack migration on OBC data: 72nd Ann. Internat. Mtg., Soc. of Expl. Geopohys., Expanded Abstracts, 1244-1247.

Thorbecke, J. W., and Rietveld, W. E. A., 1994, Optimum extrapolation operators – A comparison: 56th Ann. Internat. Mtg., Eur. Assn. Geosci. Eng., P105.

Thorbecke, J. W., Wapenaar, C. P. A. and Swinnen, G., 2004, Design of one-way wavefield extrapolation operators, using smooth functions in WLSQ optimization: Geophysics, **69**, 1037-1045.

Wapenaar, C. P. A., Fokkema, J. T. and Thorbecke, J. W., 1997, Inverse wavefield extrapolation revisited: Limitations of single- and multi-valued operators, 67th Ann. Internat. Mtg: Soc. of Expl. Geophys., 1509-1512.

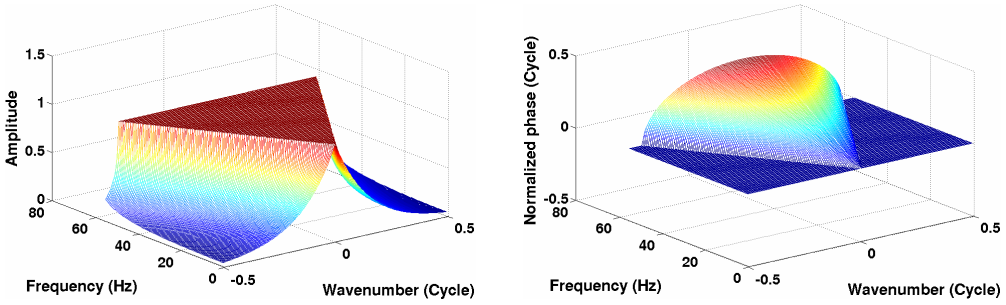

(a)

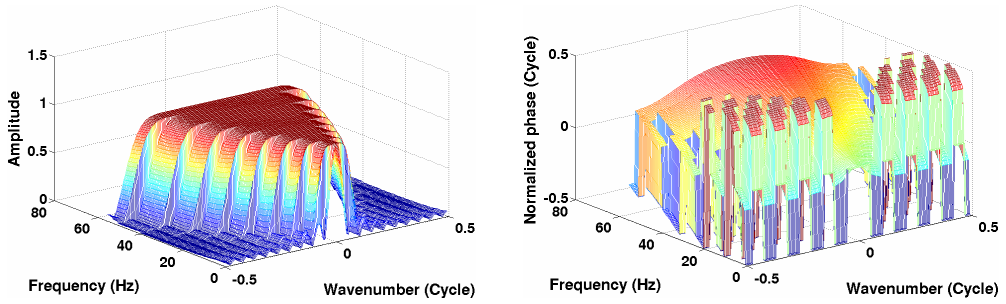

(b)

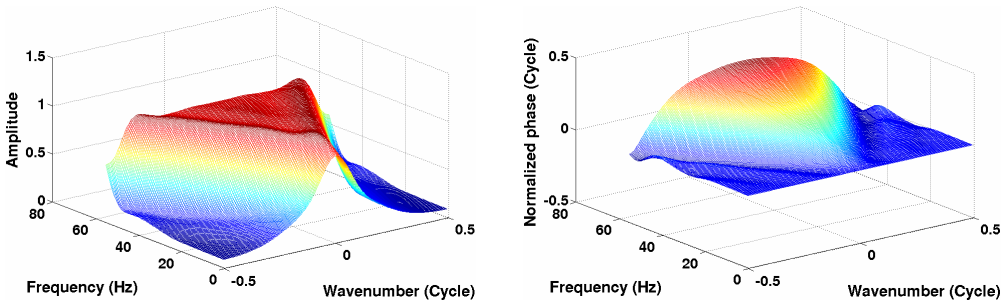

(c)

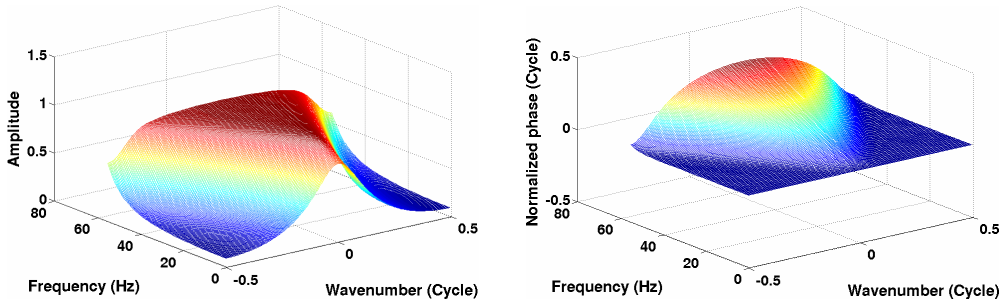

(d)

FIG. 1. 3-D visualization of various band-limited extrapolators in the wavenumber-frequency domain. Amplitude spectra are on the left, and phase spectra are on the right. (a) Desired extrapolator (from equation (1)); (b) Hale's extrapolator; (c) Kirchhoff extrapolator with a Hanning edge taper; (d) Gaussian tapered extrapolator. An operator length of 19 points is used by operators (b), (c) and (d) in the space domain.

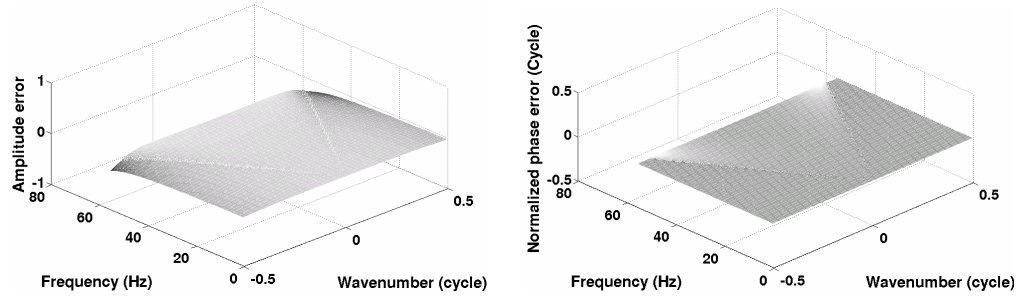

(a)

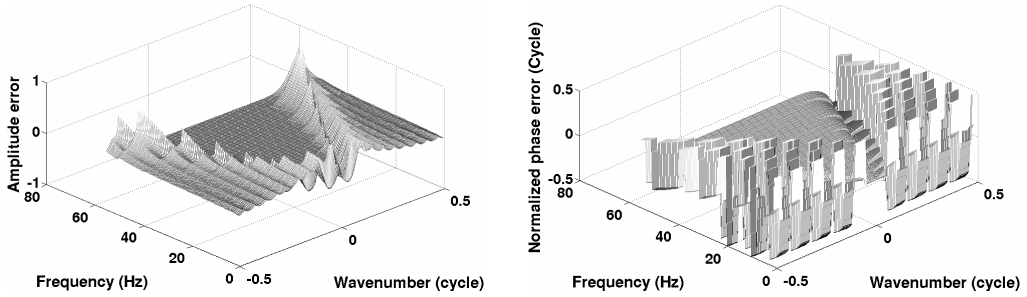

(b)

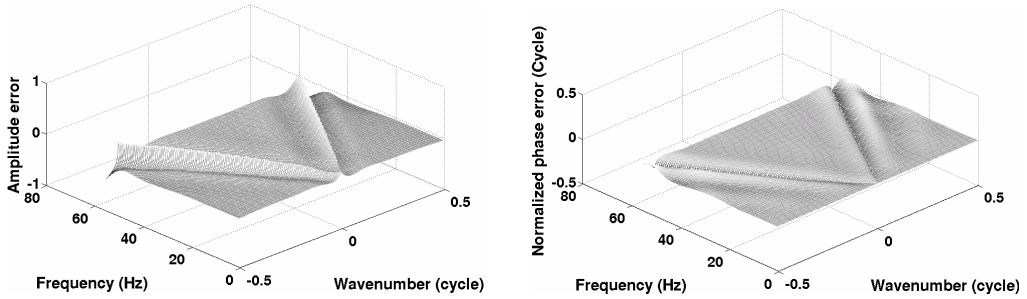

(c)

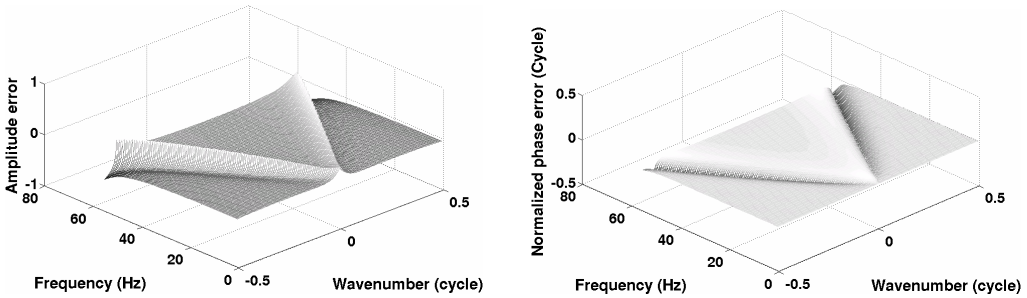

(d)

FIG. 2. Amplitude (left column) and phase (right column) errors of (a) full-aperture Kirchhoff extrapolator, (b) Hale's 19-point extrapolator, (c) 19-point Kirchhoff extrapolator with Hanning edge taper, and (d) 19-point Gaussian tapered extrapolator.

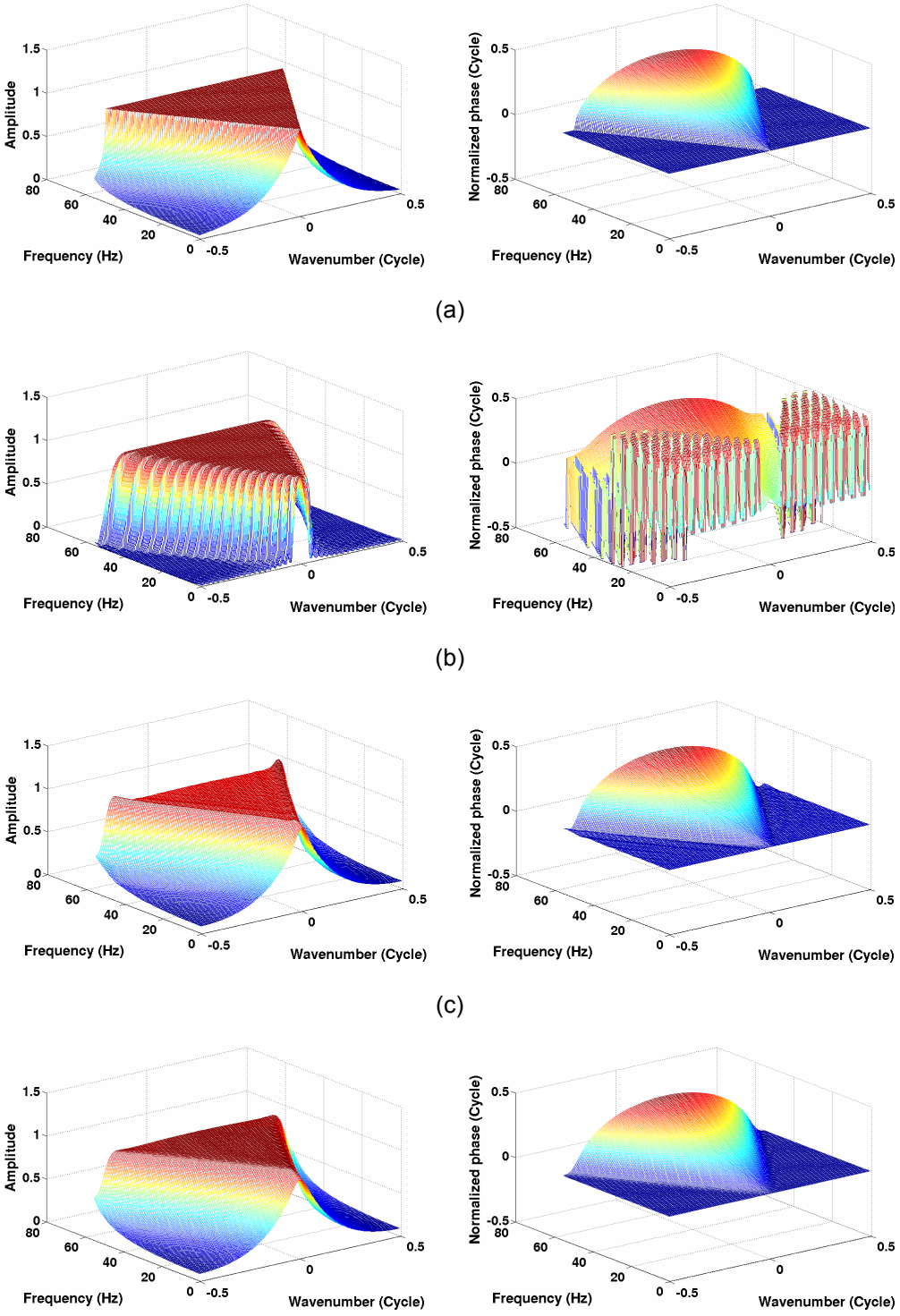

FIG. 3. 3-D visualization of various band-limited extrapolators in the wavenumber-frequency domain. The figures on the left are the amplitude spectra and on the right are the phase spectra. (a) Desired extrapolator (from equation (1)); (b) Hale's extrapolator; (c) Kirchhoff extrapolator with a Hanning edge taper; (d) Gaussian tapered extrapolator. An operator length of 39 points is used by operators (b), (c) and (d) in the space domain.

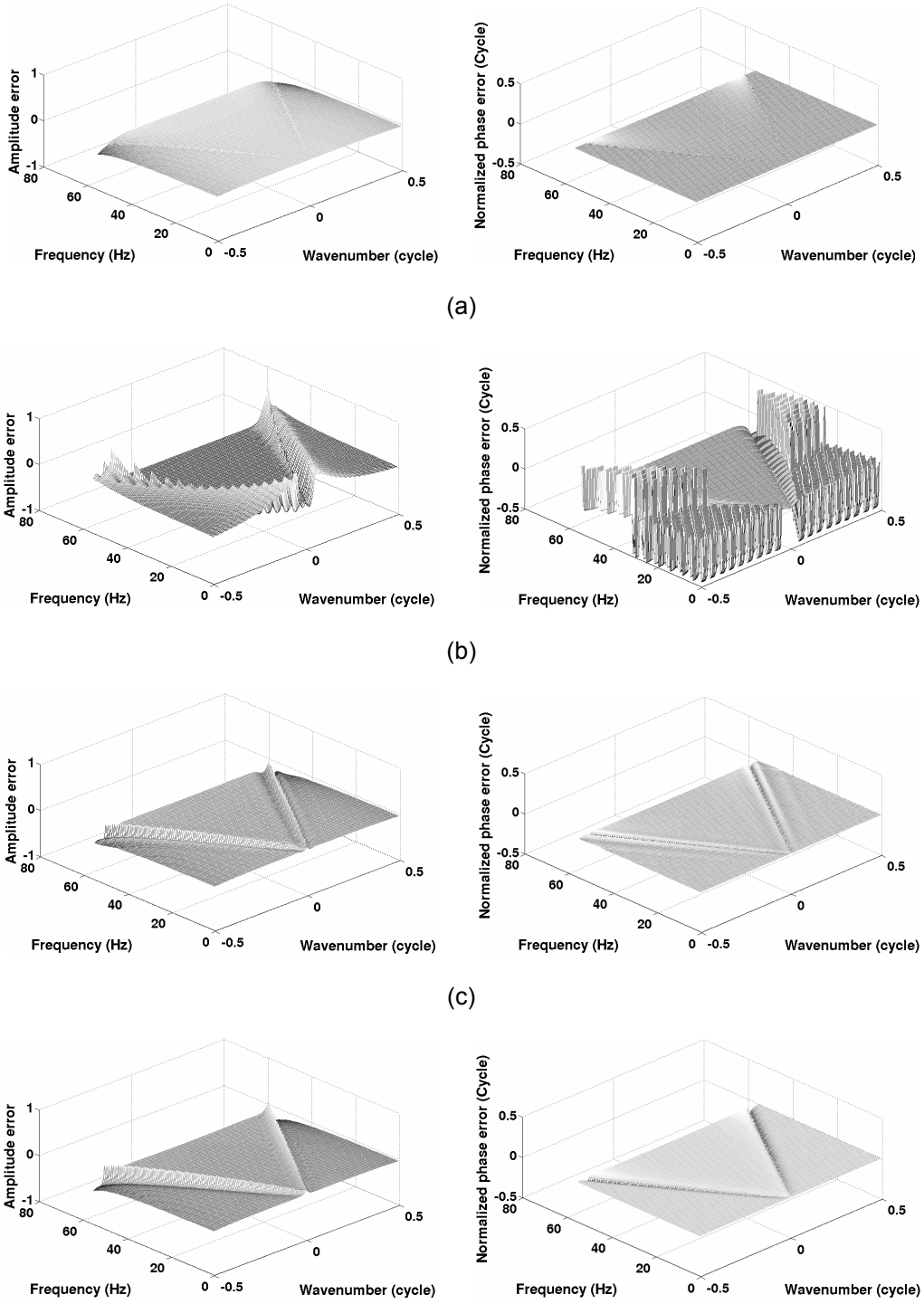

FIG. 4. Amplitude (left column) and phase (right column) errors of (a) full-aperture Kirchhoff extrapolator, (b) Hale's 39-point extrapolator, (c) 39-point Kirchhoff extrapolator with Hanning edge taper, and (d) 39-point Gaussian tapered extrapolator.

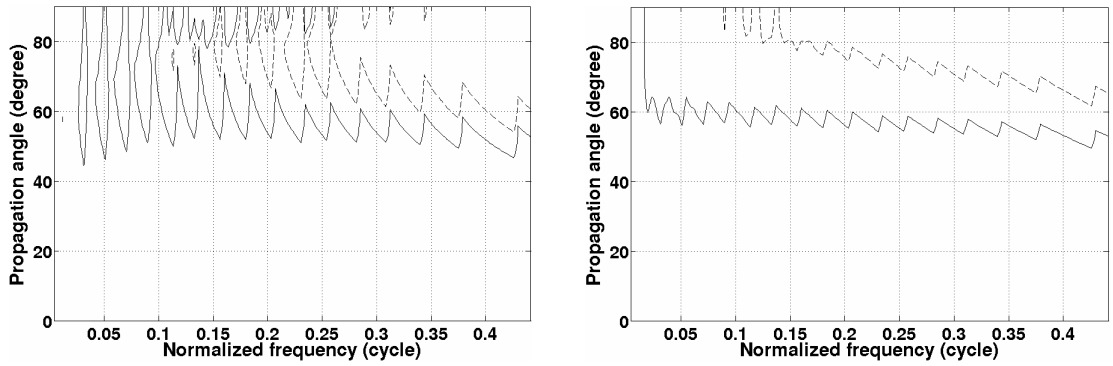

(a)

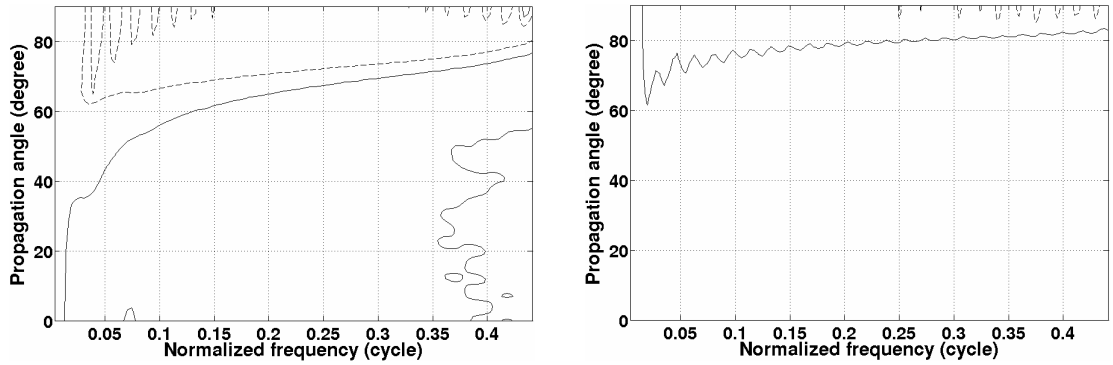

(b)

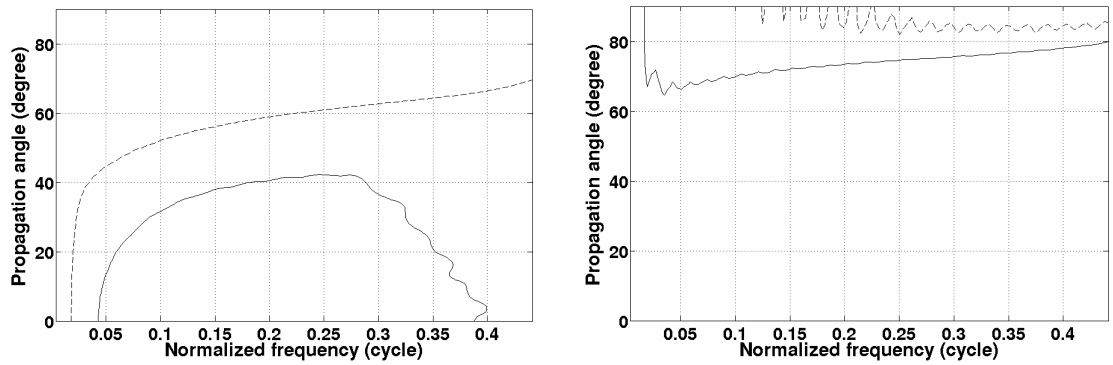

(c)

FIG. 5. Amplitude and phase error contours for (a) Hale's 39-point extrapolator, (b) 39-point Kirchhoff extrapolator with Hanning edge taper, and (c) 39-point Gaussian tapered extrapolator. Figures on the left are the contours showing amplitude error. Contour values are 1/20 (dash lines) and 1/200 (solid lines). Figures on the right are the contours showing phase error. Contour values are $-\pi/100$ (dash lines) and $-\pi/1000$ (solid lines). Frequency is normalized by multiplying dx/v.

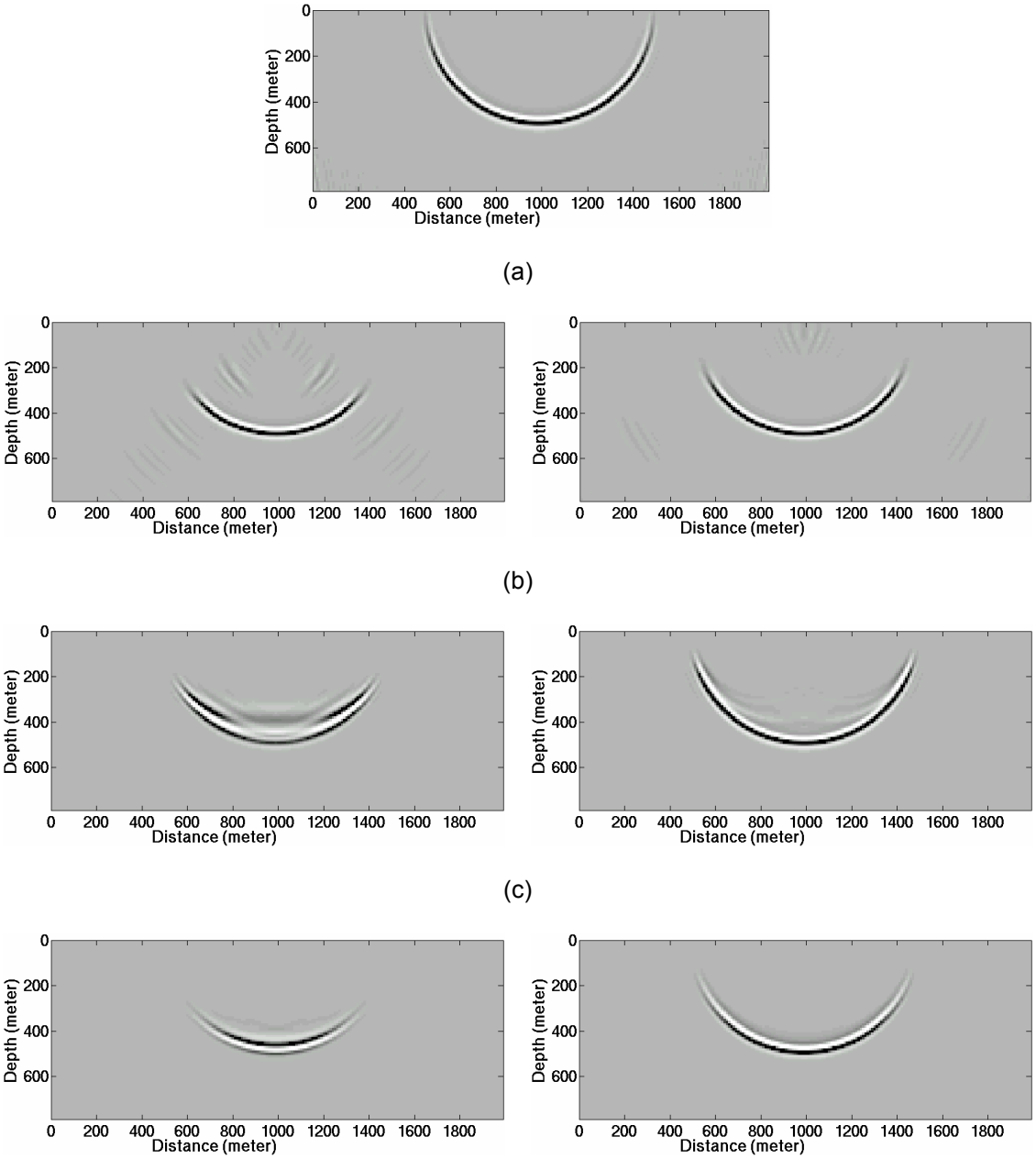

FIG. 6. Impulse responses (zero-offset migration) of (a) full-aperture Kirchhoff extrapolator, (b) Hale's 19- and 39-point extrapolators, (c) 19- and 39-point Kirchhoff extrapolators with Hanning edge taper, and (d) 19- and 39-point Gaussian tapered extrapolators. The impulse responses are computed for Δt=4ms, Δx=Δz=10m, half-velocity of 1250m/s and 200 extrapolation steps.

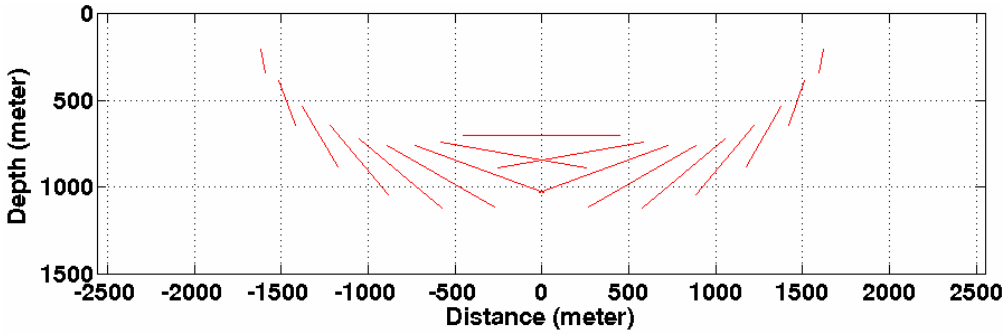

(a)

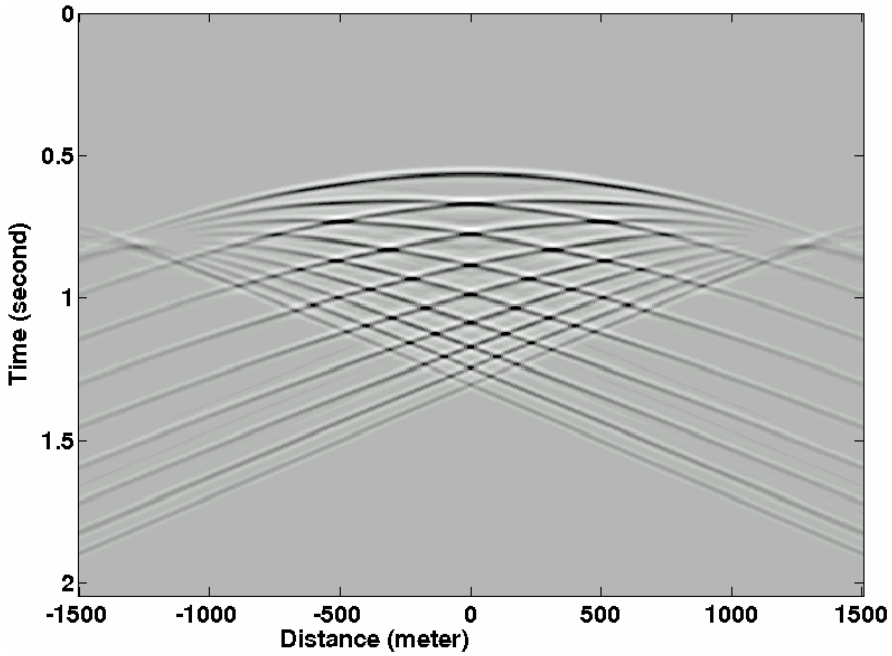

(b)

FIG. 7. (a) A constant velocity earth model containing 17 dipping events. For a better comparison, reflectors are symmetric with x=0. (b) Synthetic shot record of the model.

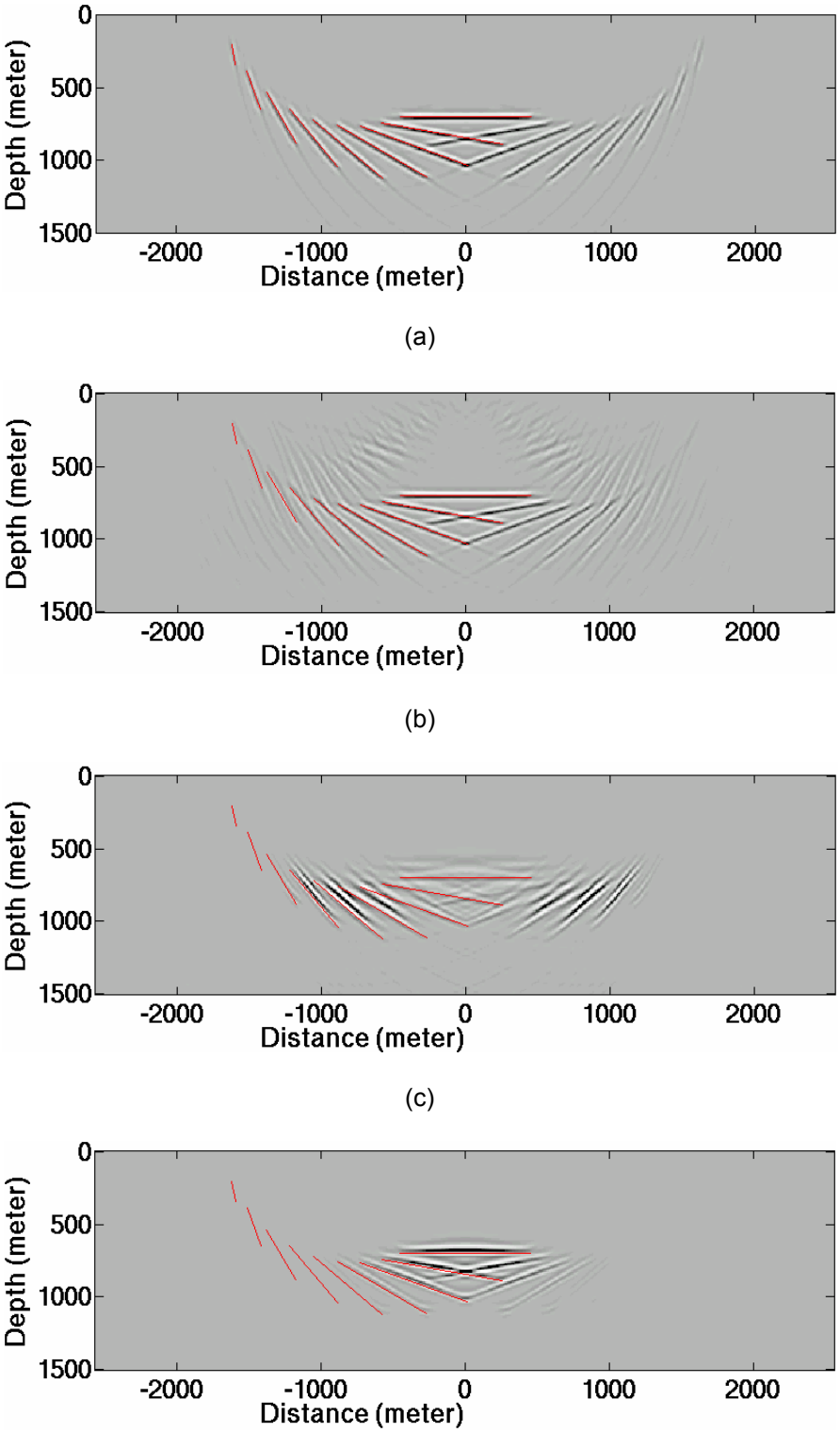

FIG. 8. Migration of pre-stack synthetic data by using (a) full-aperture Kirchhoff extrapolator, (b) Hale's 39-point extrapolator, (c) 39-point Kirchhoff extrapolator with Hanning edge taper, and (d) 39-point Gaussian tapered extrapolator.